

Non-isolated Modified Quadratic Boost Converter with Midpoint Output for Solar Photovoltaic Applications

Ravivarman *Shanmugasundaram*^{1*}, Natarajan *Karupiah*², and Raja Gopal *Reddy B*²

¹Professor, Department of Electrical and Electronics Engineering, Vardhaman College of Engineering, Hyderabad, Telangana

²Associate Professor, Department of Electrical and Electronics Engineering, Vardhaman College of Engineering, Hyderabad, Telangana

Abstract. This paper presents a boost DC-DC converter topology with non - isolated high gain and output midpoint, to boost the voltage obtained from solar photovoltaic panels. The three-level boost converter is coupled to the output port of the single-switch quadratic boost converter to derive the proposed converter topology. The voltage gain of the proposed converter is greater than that of the classical boost converter. The voltage stress on the switches of the proposed converter is equal to half of the converter output voltage. Static analysis, operating modes, experimental waveforms in continuous current conduction and discontinuous current conduction modes are shown. A 520 W prototype converter was implemented in the laboratory and its results are presented.

1 Introduction

In photovoltaic systems with multiple modules connected in series, partial shadowing can lead to a reduction of voltage and power available from the panels together. In addition, the tracking of maximum power point is complex because the system has multiple peaks, resulting from the local maximum power points. In [1, 2] a comparative investigation of various photovoltaic arrangements with partial shading is presented. Still, the power of a photovoltaic panel is between 100 W and 350 W, and the voltage at maximum power point is 12 V to 42 V. The above values are not sufficient when compared to the voltage required in the dc bus of inverters, which reduces the efficiency of the whole system [3, 4].

To extend the conversion range, the cascaded boost converters was used [5, 6]. However, the resulting structure is large and control is complex. With simplified structure, the quadratic boost converter with a single switch was proposed and analysed in [7-9], and in [9, 10] the drive cell has been associated to aid self-resonant switching, allowing the zero-voltage switching in the converter switch. The voltage gain can be increased by using magnetic coupling, coupled inductors based high gain converters are introduced in [11, 12]. With this technique, the ripples in the inductor current and the reverse recovery problems in the diodes are reduced. However, the voltage stress of the output diode is still high, the leakage inductance and parasitic capacitor of the diode will form a resonant circuit. Additionally, the ripples in the input current is highly discontinuous. By switched - capacitor technique, the topologies proposed in [13, 14] provide increased gain, but this can be achieved by using large number of capacitors.

The conduction and switching losses of quadratic converters are significant, making these converters more suitable for low power applications. Using three-state cells, high-gain converters with reduced input current ripple was proposed in [15, 16]. The solution presents a high gain, where the gain is increased by increasing the turns-ratio of the coupled inductor. A converter topology utilizing three-state cell and voltage multiplier cell was proposed in [17]. This solution may be limited to high power applications as a function of the current flowing through the capacitors. The voltage stresses in the semiconductor devices can be reduced as in [18], where the maximum voltage applied to the switches are equal to the fraction of its converter output voltage. The topology proposed in [19] presents asymmetry in the voltages across the switches when the gain is greater than 4, being characterized as a disadvantage despite the converter can operate with gains higher than four. Other quadratic converter topologies were presented in [20, 21], for driving the Light Emitting Diode, but the step-down voltage version. Besides these applications, a quadratic converter was used as a battery charger in [22]. In this case the system was developed to contemplate a high power-factor. With high voltage gain and low input current ripple, a converter topology based on interleaving technique was proposed in [23]. This article proposes a new topology for high gain DC-DC converter based on quadratic feature, which use low voltage switch and access to the midpoint of the output voltage.

The proposed converter topology is devised by connecting the three-level boost cell [24] shown in Fig. 1 (a) to the output port of the quadratic boost converters [5-7] which is shown in Fig. 1 (b). The resultant proposed converter is shown in Fig. 2.

* Corresponding author: siliconravi@yahoo.com

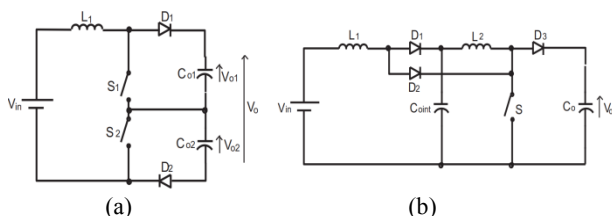


Fig. 1. Boost converter (a) Three level boost converter
 (b) Quadratic boost converter

Use In the proposed topology, an appropriate modulation strategy was adopted and the output capacitors are equal, $C_{o1} = C_{o2}$, hence the voltage on these capacitors will be half of total output voltage of converter. The switches, S_1 and S_2 are clamped at half of output voltage, thus a significant reduction in voltage stress on switches. In contrast, current flowing through the switches are the sum of the currents of inductors, L_1 and L_2 . The switching technique used for operating the proposed converter is a delayed modulation technique, implemented through two 180° lagged pulses with fixed frequency and variable duty ratio. The converter will have two distinct regions of operation, the first relating to operation where duty cycle is lesser than 0.5 and other with a duty cycle greater than 0.5. The control signals of the switches can be seen in Fig. 4 and Fig. 6.

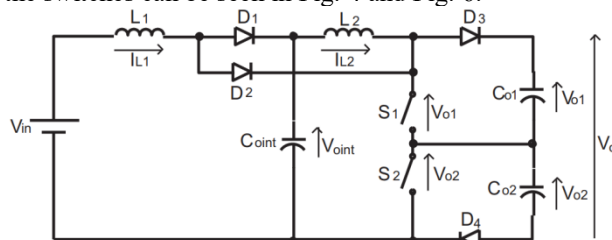


Fig. 2. Proposed boost converter

2 Principle of operation

To understand the proposed converter operation, the analysis is made for Continuous Conduction Mode (CCM) and Discontinuous Conduction Mode (DCM) operations and the converter is investigated in the two regions defined by the duty cycle ratios.

2.1 Operation in CCM The operating modes in CCM for duty ratio less than 0.5 are described below. The four operating modes of proposed converter for $D < 0.5$ is shown in Fig. 3. The theoretical waveforms related to these modes are shown in Fig. 5.

First step of operation ($t_0 - t_1$) - (Fig. 3 (a)): Switches, S_1 and S_2 are in off state and the inductor current decreases linearly. While the C_{o1} capacitor and the inductor L_1 are being charged from the input power source, the inductor L_2 and the capacitors C_{o1} and C_{o2} supply power to the load.

Second step of operation ($t_1 - t_2$) - (Fig. 3 (b)): In this step of operation, S_1 remains in off state and S_2 is switched

on. The energies from the input source and inductors are transferred to both the capacitor C_{o1} and the load.

Third step of operation ($t_2 - t_3$) - (Fig. 3 (a)): This step of operation begins when S_2 is turned off. The topological structure and the operation of this step are similar to the first step of operation.

Fourth step of operation ($t_3 - t_4$) - (Fig. 3 (c)): During this step of operation, switch S_1 is turned on and the switch S_2 remains in off state. The energy is transferred to the capacitor C_{o2} and load from the input source. From the theoretical waveforms which was shown in Fig. 4, for $D < 0.5$, the equations for time intervals in terms of duty cycle, D and time period, T are given in (1) and (2).

The voltage gain of the proposed converter in Continuous Conduction Mode for duty cycle less than 0.5 can be obtained by determining the average voltage in inductors L_1 and L_2 during one full cycle of operation. Since this converter is composed of two conversion stages, static gain analysis can be done individually.

$$\Delta t_1 = \Delta t_4 = \frac{T(1-2D)}{2} \quad (1)$$

$$\Delta t_2 = \Delta t_3 = DT \quad (2)$$

At steady state, the average inductor voltage across L_1 is equal to zero, as given by (3), where V_{in} is the input voltage; V_{o1} is the intermediate voltage and V_o is the output voltage. The partial voltage gain of the first step of operation is calculated and given in (4).

In the same way, the partial voltage gain is determined for the second step of operation, and it is given in equations (5) and (6). Multiplying the partial voltage gains (4) and (6), which gives equation (7), the total voltage-gain of the proposed converter in continuous conduction mode for $D < 0.5$.

$$2\Delta t_1 (V_{in} - V_{o1}) + \Delta t_2 (2V_{in} - V_o) = 0 \quad (3)$$

$$\frac{V_{o1}}{V_{in}} = \frac{1-D}{2D^2 - 2D + 1} \quad (4)$$

$$2\Delta t_1 (V_{o1} - V_o) + \Delta t_2 (2V_{o1} - V_o) = 0 \quad (5)$$

$$\frac{V_o}{V_{o1}} = \frac{1}{1-D} \quad (6)$$

$$G_{CCM(D<0.5)} = \frac{V_o}{V_{in}} = \frac{1}{2D^2 - 2D + 1} \quad (7)$$

The converter operating in CCM for duty cycle greater than 0.5 is described below. Fig. 4 illustrates the different operation steps and Fig. 6 shows the key waveforms of the proposed converter.

First step of operation ($t_0 - t_1$) - (Fig. 4 (a)): Switches, S_1 and S_2 are in conduction state and the inductor current increases linearly. At this stage of operation, there is no energy transfer between the source and the load. The load is being powered by capacitors C_{o1} and C_{o2} .

Second step of operation ($t_1 - t_2$) - (Fig. 4 (b)): The second operating step starts when the switch, S_2 is switched off and diodes D_1 and D_4 are in conducting state. The capacitor C_{o1} is being charged from the supply voltage V_{in} and the energy from inductor, L_1 . The inductor L_2 transfers its energy to the capacitor C_{o2} .

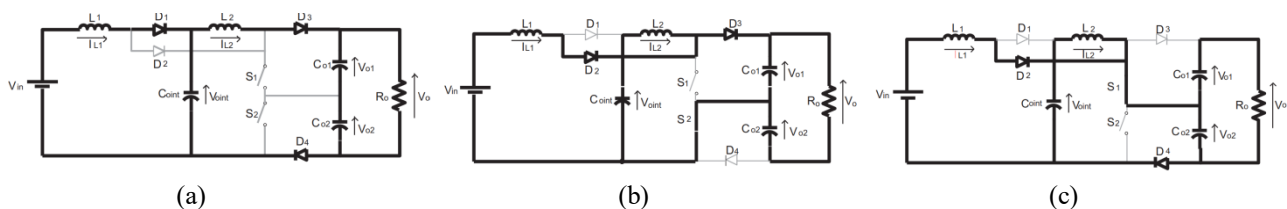


Fig. 3. Proposed boost converter operating modes in Continuous Conduction Mode ($D < 0.5$)

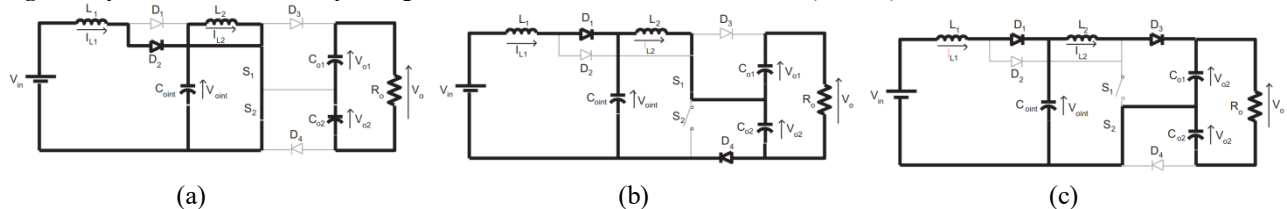


Fig. 4. Proposed boost converter operating modes in Continuous Conduction Mode ($D > 0.5$)

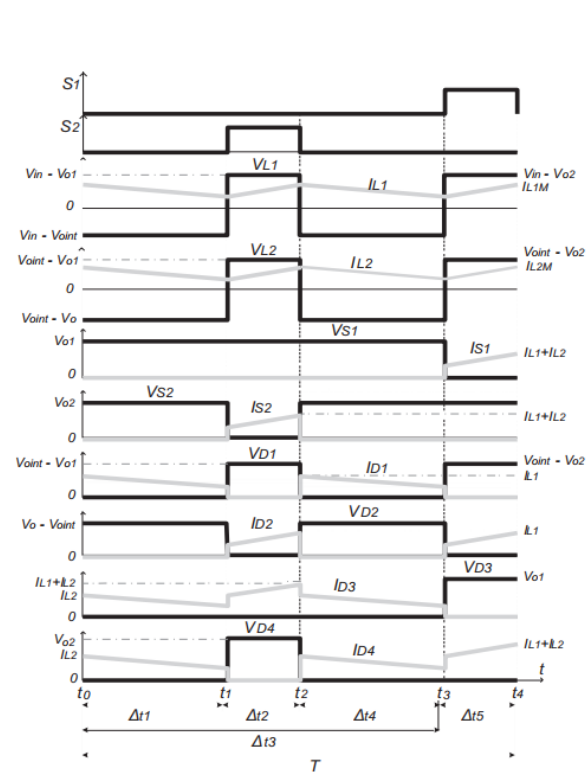


Fig. 5. Theoretical waveforms of the proposed converter in continuous conduction mode ($D < 0.5$)

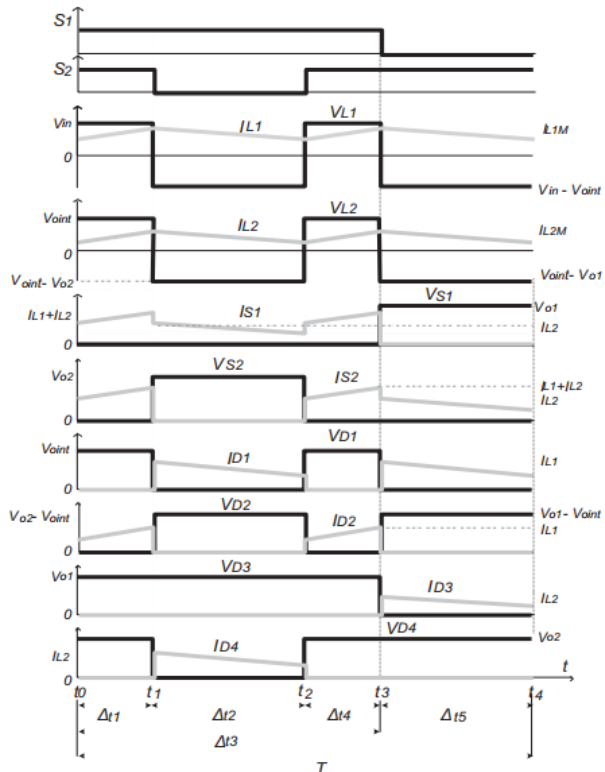


Fig. 6. Theoretical waveforms of the proposed converter in continuous conduction mode ($D > 0.5$)

Third step of operation ($t_2 - t_3$) - (Fig. 4 (a)): This step begins when S_2 is turned on again. The topological condition and operation of this step are the same as the first step of operation.

Fourth step of operation ($t_3 - t_4$) - (Fig. 4 (c)): When the switch, S_1 is turned off, the fourth step of converter operation starts. However, switch, S_2 continues its conduction process. During this operation, the power from input source, energy from L_1 , charge across C_{oint} and energy of the inductor L_2 deliver energy to the capacitor C_{o1} . The waveforms shown in Fig. 6 is used to determine

the equations of the time intervals of the four operating steps in terms of time period and duty cycle and they are given in equations (8) and (9).

$$\Delta t_1 = \Delta t_4 = \frac{T(2D-1)}{2} \quad (8)$$

$$\Delta t_2 = \Delta t_5 = T(1-D) \quad (9)$$

For $D > 0.5$, the voltage gain of the proposed converter in continuous conduction mode can be determined by analysing each operating step of converter. At steady state, the average voltage developed in the inductor, L_1 is

zero. Thus, the expression can be written as in (10). The partial voltage gain of the proposed converter in first operating step is given by the relationship between V_{in} and $V_{o\text{int}}$. It is determined by (11). In steady state, the average voltage across inductor, L_2 equals zero, as shown in (12). Equation (12) gives equation (13), which is the partial voltage gain of the proposed converter in its second operating step.

The partial voltage gains which are given in equations (11) and (13) are multiplied to determine the total voltage gain of the proposed converter in continuous conduction mode for duty cycle more than 0.5 and it is given in (14).

$$2[V_{in}\Delta t_1 + \Delta t_2(V_{in} - V_{o\text{int}})] = 0 \quad (10)$$

$$\frac{V_{o\text{int}}}{V_{in}} = \frac{1}{2(1-D)} \quad (11)$$

$$2\Delta t_1 V_{o\text{int}} + \Delta t_2(2V_{o\text{int}} - V_o) = 0 \quad (12)$$

$$\frac{V_o}{V_{o\text{int}}} = \frac{1}{1-D} \quad (13)$$

$$G_{CCM(D>0.5)} = \frac{V_o}{V_{in}} = \frac{1}{2(1-D)^2} \quad (14)$$

Fig. 7 demonstrates the voltage gain of classic boost converter, basic quadratic boost converter and the proposed converter, all operating in the continuous conduction mode. It is observed from the figure that the voltage gain of the proposed converter is always greater than (or equal at $D = 0.5$) the gain of the classic boost converter. In this way, one can obtain higher voltages from a lower voltage, without using larger duty cycles, which results in reduction of power losses in the semiconductor devices.

For a given current ripple specifications, it is possible to obtain the value of inductances L_1 and L_2 , for both the duty cycle less than 0.5 and greater than 0.5, and it is given in equations (15) to (18).

$$L_{1(D<0.5)} = \frac{V_o [4D^3 - 4D^2 + D]}{2\Delta I_{L1} f} \quad (15)$$

$$L_{2(D<0.5)} = \frac{V_o [D(1-2D)]}{2\Delta I_{L2} f} \quad (16)$$

$$L_{1(D>0.5)} = \frac{V_o [(1-D)^2(2D-1)]}{\Delta I_{L1} f} \quad (17)$$

$$L_{2(D>0.5)} = \frac{V_o [(1-D)(2D-1)]}{2\Delta I_{L2} f} \quad (18)$$

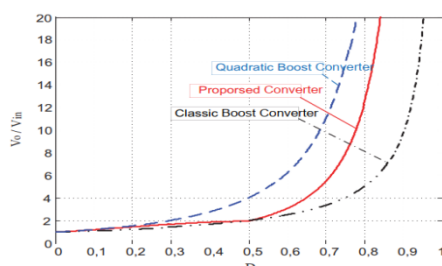


Fig. 7. Voltage gain of classic boost converter, basic quadratic boost converter and proposed converter

The equations of the current ripple in the inductor L_1 can be normalized by dividing (15) and (17) by the input current of the converter. The input current is related to output current, which results in (19) and (20). Thus, we have (21) and (23), where R_o represents load resistance. The current ripple of inductor L_2 has been normalized by dividing (16) and (18) by the output current of converter, which results in equations (22) and (24).

$$I_{in\text{med}(D<0.5)} = \frac{I_o}{2D^2 - 2D + 1} \quad (19)$$

$$I_{in\text{med}(D>0.5)} = \frac{I_o}{2(1-D)^2} \quad (20)$$

$$\frac{\Delta I_{L1(D<0.5)}}{R_o} \frac{L_1 f}{R_o} = \frac{(4D^3 - 4D^2 + D)(2D^2 - 2D + 1)}{2} \quad (21)$$

$$\frac{\Delta I_{L2(D<0.5)}}{R_o} \frac{L_2 f}{R_o} = \frac{D(1-2D)}{2} \quad (22)$$

$$\frac{\Delta I_{L1(D>0.5)}}{R_o} \frac{L_1 f}{R_o} = 2(1-D)^4(2D-1) \quad (23)$$

$$\frac{\Delta I_{L2(D>0.5)}}{R_o} \frac{L_2 f}{R_o} = \frac{(1-D)(2D-1)}{2} \quad (24)$$

The normalized relative ripple current of the inductors for the two operating regions are shown in Fig. 8. The voltage ripples in the intermediate capacitor $V_{Co\text{int}}$ and output filter capacitors V_{Co1} and V_{Co2} are determined from the expressions (25) and (26), respectively. V_{Co1} and V_{Co2} are the voltages in the output filter capacitors, I_o is the output current of the converter and f is the switching frequency of the converter.

$$\Delta V_{Co\text{int}} = \frac{2I_o(V_{o\text{int}} - V_{in})}{C_{o\text{int}} f V_{in}} \quad (25)$$

$$\Delta V_{Co1} = \Delta V_{Co2} = \frac{I_o(2V_{Co1} - V_{o\text{int}})}{2C_{o1} f V_{Co1}} \quad (26)$$

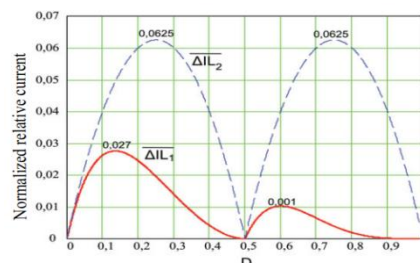


Fig. 8. Normalized relative ripple current of the inductors

2.2 Operation in DCM

In the discontinuous conduction mode, three possible discontinuities occur in the proposed converter operation. The first two possibilities are identified by the discontinuity of current in the inductor L_1 or current in the inductor L_2 . While the third possibility is indicated by the discontinuity of currents flowing in both L_1 and L_2 . The first two possibilities will be called as first Partial

Discontinuous Conduction Mode (PDCM) and the third possibility will be called as Total Discontinuous Conduction Mode (TDCM). However, considering that the mean current of L_1 is greater than the mean current of L_2 and if the current ripple in both inductors are equal, then the current flowing in inductor L_2 always cancels the current flowing in the inductor L_1 . Thus, in this work, the PDCM operation refers to the current discontinuity only in the inductor L_2 .

The analysis for the PDCM is presented for the two operating conditions defined by the duty cycle (for $D < 0.5$ and for $D > 0.5$). The six operating steps of the proposed converter in the PDCM for the duty cycle less than 0.5 are explained below. The circuit diagrams of the converter for different operation steps and the theoretical waveforms of the proposed converter are shown in Fig. 9 and Fig. 10.

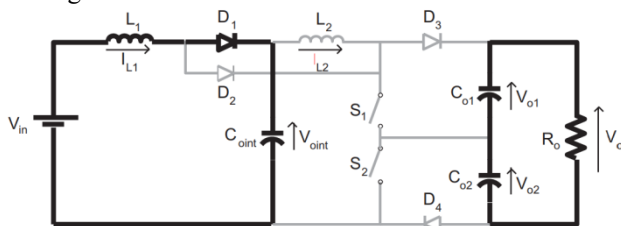


Fig. 9. Proposed boost converter operating modes in Partial Discontinuous Conduction Mode ($D < 0.5$)

First operation step ($t_0 - t_1$) - (Fig. 3 (a)): The switches, S_1 and S_2 remain in off state and the inductor current decreases linearly. While the source V_{in} and L_1 send energy to C_{oint} , the inductor L_2 and the capacitors C_{o1} and C_{o2} feed energy to the load.

Second operation step ($t_1 - t_2$) - (Fig. 9): This operation step starts when the current of L_2 reaches zero, blocking D_3 and D_4 . In this step, the C_{oint} capacitor continues to be charged with the energy of V_{in} and L_1 , however the load is fed by the capacitors C_{o1} and C_{o2} .

Third operation step ($t_2 - t_3$) - (Fig. 3 (b)): When the switch S_2 is turned on and switch S_1 remains in off state, this third step of operation starts. The current flowing through the inductors L_1 and L_2 increases linearly, and energy is transferred to C_{o1} and the load.

Fourth operation step ($t_3 - t_4$) - (Fig. 3 (a)): During this operation step, switches S_1 and S_2 are in off state. The topological condition and operation of this step are the same as first mode.

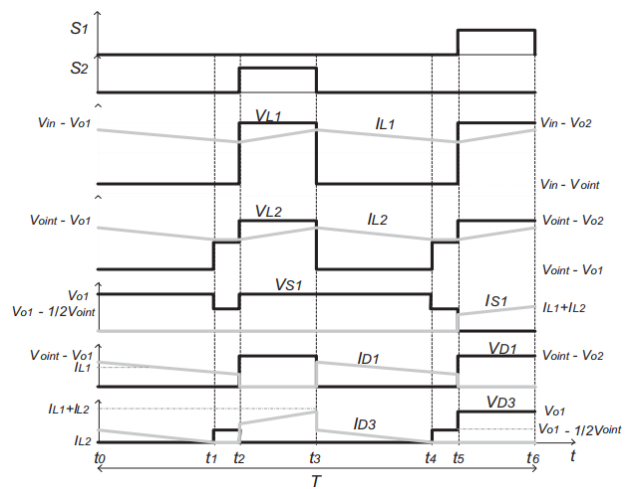


Fig. 10. Theoretical waveforms of the proposed converter in partial discontinuous conduction mode ($D < 0.5$)

Fifth operation step ($t_2 - t_3$) - (Fig. 9): This mode of operation starts, when the L_2 current reaches zero. The topological condition and operation of this step are the same as the second step of operation.

Sixth operation step ($t_3 - t_4$) - (Fig. 3 (c)): In this operation step, the switch S_1 is turned on, and switch S_2 remains in off state. During this operating mode, current flowing through the inductors L_1 and L_2 increase again. The capacitor C_{o2} and the load receives the energy from the inductors.

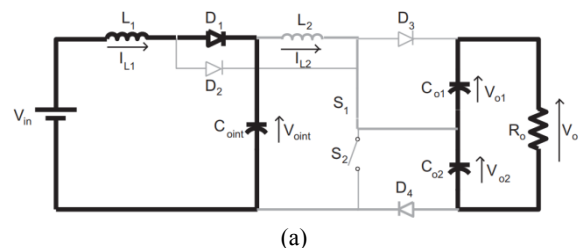
The six converter operating steps in PDCM for duty cycle greater than 0.5 are described below. The converter operating modes and the theoretical waveforms are shown in Fig. 11 and Fig. 12.

First step of operation ($t_0 - t_1$) - (Fig. 5 (a)): In this mode of operation, the switches S_1 and S_2 are in conducting state and the current flowing through the inductors increases linearly. D_1 , D_3 and D_4 are in off state. The load is being powered by the capacitors C_{o1} and C_{o2} .

Second operation stage ($t_1 - t_2$) - (Fig. 5 (b)): In this operating step S_1 remains conducting and S_2 is turned off. The currents in the inductors decrease linearly. The source V_{in} and inductor L_1 transfers the energy to C_{oint} , however L_2 transfers the energy to C_{o2} and load.

Third operation step ($t_2 - t_3$) - (Fig. 11 (a)): This stage begins when the L_2 current reaches zero, reverse biasing D_3 and D_4 . The supply voltage V_{in} and the inductor L_1 charges C_{oint} continues to charge with the energy obtained from V_{in} and L_1 , and the load is fed by the capacitors C_{o1} and C_{o2} .

Fourth operation phase ($t_3 - t_4$) - (Fig. 5 (a)): this operation mode starts when S_2 is turned on again. In this step, the inductors store energy and capacitors C_{o1} and C_{o2} feed the load.



(a)

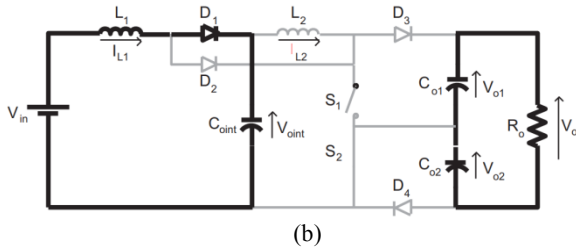


Fig. 11. Proposed boost converter operating modes in Partial Discontinuous Conduction Mode ($D > 0.5$)

Fifth stage operation ($t_4 - t_5$) - (Fig. 5 (c)): When the switch S_1 is turned off, the converter shifts to this operating mode. In this mode, the source V_{in} and L_1 charge the capacitor C_{o1} , while the inductor L_2 delivers the energy to C_{o1} and the load.

Sixth stage operation ($t_5 - t_6$) - (Fig. 11 (b)): This mode occurs when the current in L_2 reaches zero, and the diode D_3 is reverse biased. The topological state and operation of this step are similar to the third step.

Based on the converter operating mode waveforms shown in Fig. 10 and Fig. 12, the mean values of the voltages in the inductors L_1 and L_2 are calculated, we obtain (27) and (28), which gives the equations for the total voltage gain of the proposed converter in partial discontinuous conduction mode. The parameter γ_2 is a current parameter which represents the external factors that influence the static behaviour of the converter.

$$G_{PDCM(D<0.5)} = \left[1 + \frac{D^2}{\gamma_2(1-2D)} \right] \left[\frac{1-D}{2D^2-2D+1} \right] \quad (27)$$

$$G_{PDCM(D>0.5)} = \left[2 + \frac{(2D-1)^2}{\gamma_2} \right] \left[\frac{1}{2(1-D)} \right] \quad (28)$$

3. Experimental results

A laboratory prototype of the proposed converter with a power rating of 520 W was built in order to demonstrate its operation and performance. The parameters used to design the proposed converter is given in Table 1. The power rating and rated voltage values are equal to an array of four solar photovoltaic panels, each having 130W and 17 V at maximum power. The switching frequency was chosen with the purpose of comparing the constructive aspects of this converter with the work carried out in [19]. The design parameters of the inductors and the capacitors presented in the proposed converter were calculated by considering the duty cycle, $D = 0.79$. The maximum current ripples of the inductors were limited to 20% of the mean value of the current in each inductor. The voltage ripples on the capacitors were limited to 1% of the mean voltage on the respective capacitor.

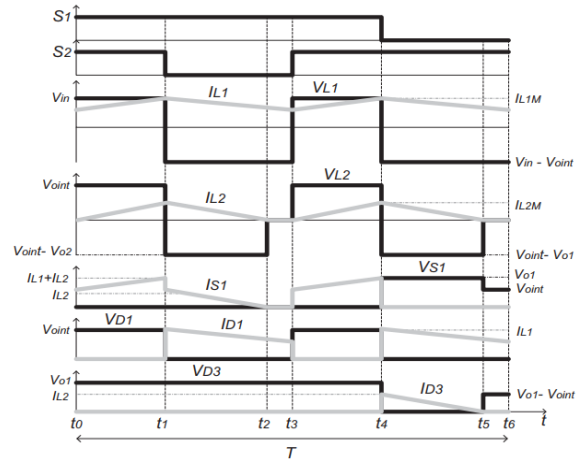
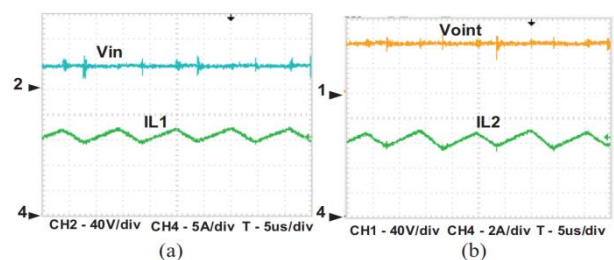


Fig. 12. Theoretical waveforms of the proposed converter in partial discontinuous conduction mode ($D > 0.5$)

Table 1. Selection of Proposed Converter Parameters.

Design Considerations	Selected Values
Rated power, P_o	520 W
Input voltage, V_{in}	34 V
Output voltage, V_o	380 V
Switching frequency, f	50 kHz

Fig. 13 shows the experimental waveforms of the proposed converter. The input voltage is 34 V and the mean current flowing through the inductor is 15.38 A with ripple of 9 %, which is allowable as shown in Fig. 13 (a). The intermediate voltage across the capacitor is almost 80 V and the mean current flowing through the inductor L_2 is 6.47 A, with ripple of 12 % as shown in Fig. 13 (b). The voltage stress across the switches S_1 and S_2 and maximum reverse blocking voltage across the diodes D_3 and D_4 are 190 V, which is equal to half of the total output voltage of the converter as shown in Fig. 13 (c) and 13 (d). The proposed converter has midpoint in the output port, so that the inverter can be directly connected to it without using any extra components. The voltage across each output capacitor is equal to 190 V as shown in Fig. 13 (e). The output voltage and current of the proposed converter for given specification is shown in Fig. 13 (f), and they are 380 V and 1.37 A, respectively. Fig. 14 shows the efficiency curve of the converter as a function of output power. The efficiency reaches its maximum value at the output power of 350W. Although the efficiency value is low when compared to other single-stage and high-voltage converters, similar results were found in other high gain and low input voltage converters.



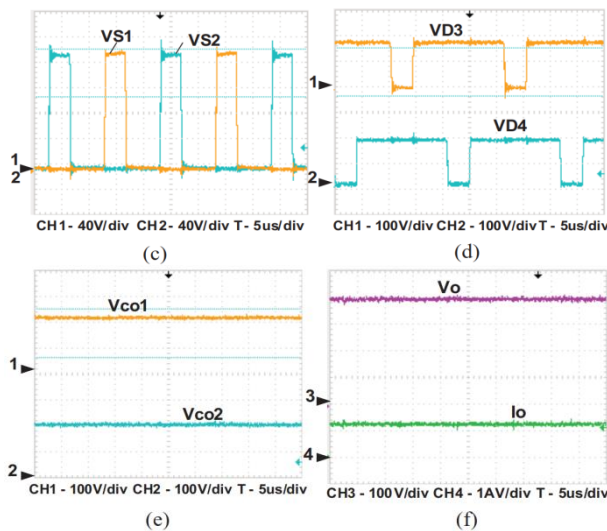


Fig. 13. Experimental waveforms of the proposed converter

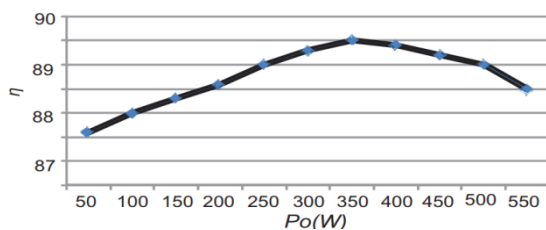


Fig. 14. Efficiency – output power characteristics of the proposed boost converter

References

1. R. D. de Oliveira Reiter, L. Michels, J. R. Pinheiro, R. A. Reiter, S. V. G. Oliveira, A. Péres, Comparative analysis of series and parallel photovoltaic arrays under partial shading conditions, *2012 10th IEEE International Conference on Industry Applications, Fortaleza*, pp. 1-5, (2012)
2. C. T. K. Kho, J. Ahmed, S. Kashem, Y. L. Then, A comprehensive review on PV configurations to maximize power under partial shading, *TENCON 2017 - 2017 IEEE Region 10 Conference, Penang*, pp. 763-768, (2017)
3. S. M. Chen, T. J. Liang, L. S. Yang, J. F. Chen, A Safety Enhanced, High Step-Up DC–DC Converter for AC Photovoltaic Module Application, *IEEE Trans. on Power Electronics*, (27) 4, pp. 1809-1817, (2012)
4. F. L. Tofoli, D. d. C. Pereira, W. Josias de Paula, D. d. S. Oliveira Júnior, Survey on non-isolated high-voltage step-up dc–dc topologies based on the boost converter, *IET Power Electronics*, (8) 10, pp. 2044-2057, (2015)
5. M. Lotfi Nejad, B. Poorali, E. Adib, A. A. Motie Birjandi, New cascade boost converter with reduced losses, *IET Power Electronics*, (9) 6, pp. 1213-1219, (2016)
6. J. Lu, Y. Wang, X. Li, Isolated high step-up DC–DC converter with integrated cascade structure, *IET Power Electronics*, (11) 7, pp. 1143-1152, (2018)
7. D. Maksimovic, S. Cuk, Switching converters with wide DC conversion range, *IEEE Transactions on Power Electronics*, (6) 1, pp. 151-157, (1991)
8. Tsai-Fu Wu, Te-Hung Yu, Unified approach to developing single-stage power converters, *IEEE Transactions on Aerospace and Electronic Systems*, (34) 1, pp. 211-223, (1998)
9. L. H. S. C. Barreto, E. A. A. Coelho, V. J. Farias, L. C. de Freitas, J. B. Vieira, An optimal lossless commutation quadratic PWM Boost converter, *APEC. Seventeenth Annual IEEE Applied Power Electronics Conference and Exposition, Dallas, TX*, (2), pp. 624-629, (2002)
10. S. Sharifi, M. Jabbari, H. Farzanehfard, A New Family of Single-Switch ZVS Resonant Converters, *IEEE Transactions on Industrial Electronics*, (64) 6, pp. 4539-4548, (2017)
11. E. S. Hass, F. C. Corrêa, C. B. Nascimento, A novel non-isolated high DC-DC voltage based on boost converter employing coupled inductor, *2017 Brazilian Power Electronics Conference (COBEP), Juiz de Fora*, pp. 1-6, (2017)
12. H. Moradi Sizkoohi, J. Milimonfared, M. Taheri, S. Salehi, High step-up soft-switched dual-boost coupled-inductor-based converter integrating multipurpose coupled inductors with capacitor-diode stages, *IET Power Electronics*, (8) 9, pp. 1786-1797, (2015)
13. O. Abutbul, A. Gherlitz, Y. Berkovich, A. Ioinovici, Step-up switching-mode converter with high voltage gain using a switched-capacitor circuit, *IEEE Transactions on Circuits and Systems I: Fundamental Theory and Applications*, (50) 8, pp. 1098-1102, (2003)
14. E. H. Ismail, M. A. Al-Saffar, A. J. Sabzali, High Conversion Ratio DC–DC Converters With Reduced Switch Stress, *IEEE Transactions on Circuits and Systems I: Regular Papers*, (55) 7, pp. 2139-2151, (2008)
15. G. V. T. Bascope, I. Barbi, Generation of a family of non-isolated DC-DC PWM converters using new three-state switching cells, *2000 IEEE 31st Annual Power Electronics Specialists Conference. Conference Proceedings, Galway*, (2) pp. 858-863, (2000)
16. R. P. Torrico-Bascopé, L. F. Costa, G. V. Torrico-Bascopé, Generation of new nonisolated high voltage gain DC-DC converters, *2011 IEEE 33rd International Telecommunications Energy Conference (INTELEC), Amsterdam*, pp. 1-8, (2011).
17. R. P. Torrico-Bascopé, F. L. Tofoli, C. G. Castelo Branco, C. M. T. Cruz, Three-state switching cell (3SSC)-based non-isolated dc–dc boost-type converter with balanced output voltage and wide voltage conversion range, *IET Power Electronics*, (11) 7, pp. 1217-1223, (2018)
18. X. Hu, G. Dai, L. Wang, C. Gong, A Three-State Switching Boost Converter Mixed With Magnetic Coupling and Voltage Multiplier Techniques for High Gain Conversion, *IEEE Transactions on Power Electronics*, (31) 4, pp. 2991-3001, (2016)

19. Y. R. de Novaes, A. Rufer, I. Barbi, A New Quadratic, Three-Level, DC/DC Converter Suitable for Fuel Cell Applications, *2007 Power Conversion Conference - Nagoya, Nagoya*, pp. 601-607, (2007).
20. T. Yan, J. Xu, X. Liu, G. Zhou, J. Gao, Flicker-free transformerless LED driving circuit based on quadratic buck PFC converter, *Electronics Letters*, (**50**) 25, pp. 1972-1974, (2014)
21. J. M. Alonso, J. Viña, D. Gacio, L. Campa, G. Martínez, R. Osorio, Analysis and design of the quadratic buck-boost converter as a high-power-factor driver for power-LED lamps, *IECON 2010 - 36th Annual Conference on IEEE Industrial Electronics Society*, pp. 2541-2546, (2010)
22. V. F. Pires, D. Foito, A. Cordeiro, A DC-DC Converter With Quadratic Gain and Bidirectional Capability for Batteries/Supercapacitors, *IEEE Transactions on Industry Applications*, (**54**) 1, pp. 274-285, (2018)
23. R. Gules, L. L. Pfitscher, L. C. Franco, An interleaved boost DC-DC converter with large conversion ratio, *2003 IEEE International Symposium on Industrial Electronics*, (**1**), pp. 411-416, (2003)
24. D. Maksimovic, R. Erickson, Universal-input, high-power-factor, boost doubler rectifiers, *Applied Power Electronics Conference and Exposition, 1995. APEC '95. Conference Proceedings 1995., Tenth Annual, Dallas, TX*, (**1**), pp. 459-465, (1995).